Sub-bandgap defect states in polycrystalline hafnium oxide and their suppression by admixture of silicon

N. V. Nguyen,[a)] Albert V. Davydov, and Deane Chandler-Horowitz
National Institute of Standards and Technology, Gaithersburg, Maryland 20899

Martin M. Frank
IBM Thomas J. Watson Research Center, Yorktown Heights, New York 10598

The crystallinity of atomic layer deposition hafnium oxide was found to be thickness dependent, with the thinnest films being amorphous and thick films being at least partially crystalline. Hafnium oxide films fabricated by metalorganic chemical vapor deposition are mostly monoclinic. Formation of hafnium silicate by admixture of 20% Si prevents crystallization. Electronic defects are reflected by an absorption feature 0.2–0.3 eV below the optical bandgap. These defects arise in polycrystalline, but not in amorphous, hafnium-based oxides. © *2005 American Institute of Physics*.
[DOI: 10.1063/1.2126136]

Over the last several years, extensive research efforts have been devoted to the development of high-permittivity ("high-*k*") dielectric materials to replace the SiO_2 gate dielectric in future generations of metal-oxide-semiconductor (MOS) field-effect transistors.[1] High-quality hafnium oxide (HfO_2) and hafnium silicate (denoted herein as HfSiO for short, although the stoichiometry may vary) have been singled out as promising materials with potentially good electrical performance.[2] However, to optimize these materials, their quality must be well controlled. For example, it has been shown that Frenkel–Poole hopping via trapping sites in HfO_2 may contribute to gate leakage in HfO_2/SiO_2 gate stacks.[3] These trapping sites are located a few tenths of an eV below the HfO_2 conduction-band edge. Herein, we report optical absorption data that shows defect states at similar energy, originating from polycrystalline, but not from amorphous, films.

Three sets of Hf-based films, each having four nominal thicknesses of 5, 10, 20, and 40 nm, were used (see Table I). 11 Å thick SiON films were first grown on 200 mm Si(100) wafers (*n* type, ~ 1 Ω cm, 800 μm thick) by an SC-1/SC-2/HF-type surface clean, followed by thermal oxynitridation using NO. Atomic layer deposition (ALD) and metalorganic chemical vapor deposition (MOCVD), the two most commonly employed deposition methods, were then used for HfO_2 and HfSiO (Hf:Si $\sim$ 80:20) growth on the SiON-coated Si substrates. Atomic layer deposition was carried out using alternating exposures of the common precursors $HfCl_4$ and H_2O in an N_2 carrier gas. Metalorganic chemical vapor deposition of HfO_2 was performed using hafnium tetra-*tert*-butoxide [HTB, $Hf(OC(CH_3)_3)_4$] and O_2;[4] for HfSiO growth, SiH_4 was additionally used as the silicon source.[5]

Vacuum ultraviolet spectroscopic ellipsometry (VUV-SE) measurements were performed on a J. A. Woollam™ ellipsometer.[6] The dielectric functions $\varepsilon = \varepsilon_1 + i\varepsilon_2$, where ε_1 and ε_2 are the real and imaginary part of ε, respectively, were determined from the analysis of ellipsometric data.[7] Infrared (IR) measurements were performed at room temperature in an evacuated Bomem DA-8 Fourier-transform infrared (FTIR) spectrometer.[6] The absorbance measurement

was enhanced by the use of a hemispherical Ge attenuation total reflection (ATR) crystal. X-ray diffraction (XRD) spectra were obtained on Bruker-AXS D8 general area detector diffraction system with Cu $K\alpha$ radiation.[6] Two-dimensional $2\theta-\chi$ patterns were collected in the 2θ range from 15° to 48° and integrated in χ to obtain the patterns.

First, we determine the degree of HfO_2 and HfSiO crystallinity using IR spectroscopy and XRD. Figure 1 displays the IR spectra for all samples. Turning first to the MOCVD HfO_2 films, prominent phonon modes are observed at ~ 685 cm^{-1} and at $\approx 770–780$ cm^{-1}. The second peak is attributed to a characteristic phonon mode of monoclinic HfO_2, as recently predicted in a theoretical study[8] (~ 779 cm^{-1}) and as observed, e.g., for thick MOCVD HfO_2 films grown from HTB (~ 750 cm^{-1}) by Frank *et al.*[9] and for HfO_2 films made by chemical solution deposition ~ 752 cm^{-1}.[10,11] A similar peak at ~ 745 cm^{-1} was identified with the crystalline phase in HfO_2 films when annealed at high temperature.[12] This clearly shows that our MOCVD HfO_2 films contain a substantial fraction of polycrystalline material. The first peak at ~ 685 cm^{-1}, by contrast, is consistent with modes of both monoclinic and amorphous HfO_2 and therefore does not allow clear phase identification.[11]

We now turn to ALD HfO_2 and MOCVD HfSiO. Interestingly, for ALD HfO_2, a prominent peak at ~ 760 cm^{-1} is only seen for the thickest 40 nm film. This must be attributed to a thickness-dependent crystallinity of ALD HfO_2, the thinnest films beings amorphous and thick films being at least partially crystalline. For MOCVD HfSiO, at all thicknesses, no signal at 760–780 cm^{-1} is observed. We conclude that all HfSiO films are amorphous, demonstrating that the incorporation of 20% Si in the Hf-based oxide prevents crystallization in as-deposited films.

The presence of crystalline or amorphous phases as determined from IR data was further confirmed by the XRD measurements (Fig. 2). XRD spectra for the MOCVD HfO_2 series indicate that these films are monoclinic with preferred (111) orientation [see Fig. 2(a) for 40 nm film]. The 40 nm ALD HfO_2 film similarly contains a (111)-textured monoclinic phase. In addition, a peak at $2\theta=30.4°$ corresponds to the (211) reflection of orthorhombic or tetragonal HfO_2 [Fig. 2(b)]. This same peak has been also reported by others for ALD HfO_2 films.[13,14] The 20 nm ALD HfO_2 film is mostly

---

a)Electronic mail: nhan.nguyen@nist.gov

TABLE I. Phase, defect state energy, optical band gap, and IR phonon frequency, as determined by VUV-SE and ATR-FTIR.

Samples	Phase	E_{def} (eV)	E_g (eV)	Mode A (cm^{-1})	Mode B (cm^{-1})
ALD - HfO$_2$, 5 nm	Amorphous		5.61	702	
ALD - HfO$_2$, 10 nm	Amorphous		5.62	692	
ALD - HfO$_2$, 20 nm	Slightly polycrystalline	5.58	5.70	685	766
ALD - HfO$_2$, 40 nm	Polycrystalline	5.60	5.80	685	758
MOCVD - HfO$_2$, 5 nm	Polycrystalline	5.55	5.85	687	783
MOCVD - HfO$_2$, 10 nm	Polycrystalline	5.60	5.90	683	781
MOCVD - HfO$_2$, 20 nm	Polycrystalline	5.60	5.90	685	777
MOCVD - HfO$_2$, 40 nm	Polycrystalline	5.60	5.85	687	768
MOCVD - HfSiO, 5 nm	Amorphous		5.80	702	
MOCVD - HfSiO, 10 nm	Amorphous		5.75	700	
MOCVD - HfSiO, 20 nm	Amorphous		5.75	694	
MOCVD - HfSiO, 40 nm	Amorphous		5.72	692	

amorphous with small amounts of monoclinic and orthorhombic or tetragonal HfO$_2$ present, while the thinnest ALD HfO$_2$ films are purely amorphous (spectra not shown here). XRD spectra for the MOCVD HfSiO series show that these samples are amorphous [Fig. 3(c)].

We now turn to the VUV-SE measurements, which provide information both about film crystallinity and electronic structure. Figure 3 displays the imaginary part ε_2 of the dielectric function for the ALD HfO$_2$ film series. At film thicknesses of 5–10 nm, a broad featureless spectrum is characteristic of amorphous materials [Figs. 3(a) and 3(b)].[15] At thicknesses of 20–40 nm, a relatively sharp feature at ~7.3 eV indicates a transition to a polycrystalline phase, consistent with the IR and XRD findings [Figs. 3(c) and 3(d)]. A similar spectral and phase transformation with film thickness was also observed for ALD ZrO$_2$ films.[16] For MOCVD and ALD HfO$_2$, VUV-SE crystallinity data is con-

sistent with the FTIR and XRD results (not shown). All experimental techniques therefore agree on the level of crystallinity of the films studied, as summarized in Table I.

Finally, we correlate film morphology to the band edge density of states, in particular the bandgap energy (E_g) and the appearance of defect states (herein, designated as E_{def}) below the band edge. As shown in Fig. 3, 5–10 nm ALD HfO$_2$ films exhibit a relatively sharp onset of the conduction band. In contrast, for 20–40 nm films, an additional feature at ~5.8 eV is observed [see the insets in Figs. 3(c) and 3(d)]. The dielectric functions of the amorphous HfO$_2$ and HfSiO samples also exhibit a small band tail below the gap [see the insets of Fig. 3(a) and 3(b)]. This weak absorption is attributed to the Urbach tail which exists below the bandgap of amorphous materials due to the disorder of the amorphous network.[17] We determine E_g and E_{def} for all HfO$_2$ and HfSiO films from VUV-SE data by plotting the empirical expression $[n(h\nu)\alpha(h\nu)h\nu]^{1/2}$ versus $h\nu$, where n, α, and $h\nu$ are the index of refraction, the absorption coefficient, and the photon energy, respectively.[15,17] It was found that this expression exhibits a linear relationship with $h\nu$ near the band edge, and therefore E_g and E_{def} can be accurately determined by extrapolation to zero (see the insets of Fig. 3). The extracted values are listed in Table I. The average values of E_g, with an
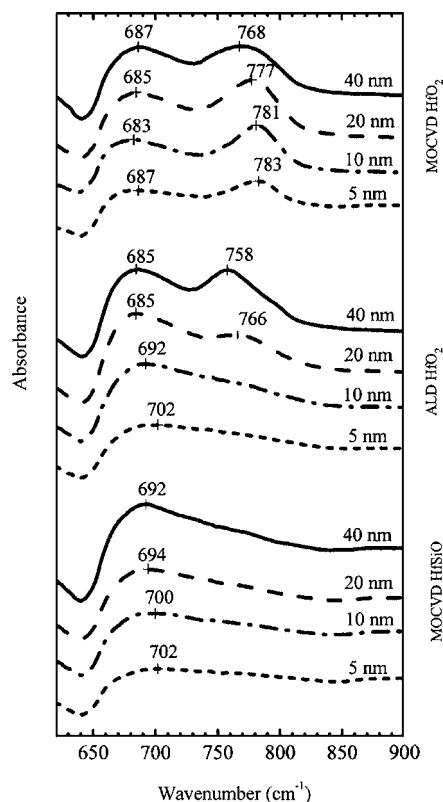

FIG. 1. IR absorption measured by enhanced sensitivity ATR-FTIR. Excellent signal-to-noise was obtained by using Germanium ATR.
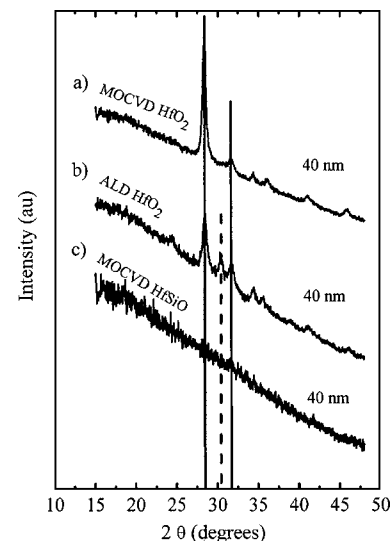

FIG. 2. XRD spectra for (a) 40 nm MOCVD HfO$_2$, (b) 40 nm ALD HfO$_2$, and (c) 40 nm MOCVD HfSiO. Spectra for 10 nm and 20 nm thick films are similar to the respective 40 nm film spectra. 5 nm ALD HfO$_2$ films are too thin to observe any reflections.
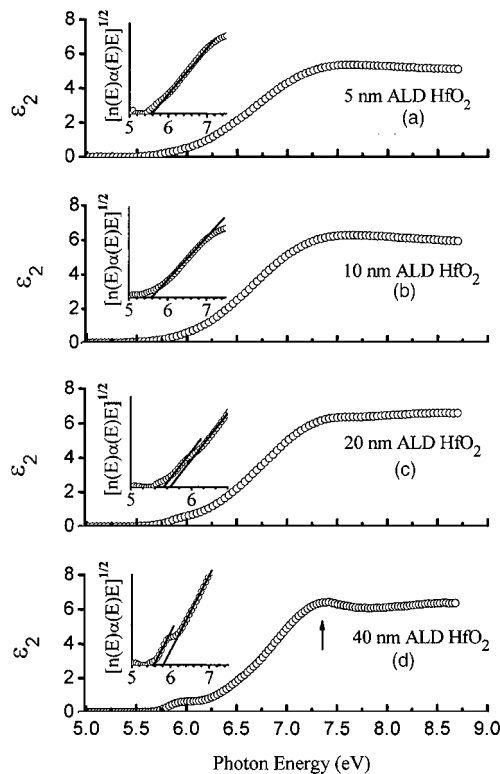
FIG. 3. The imaginary part of the dielectric function, determined from VUV-SE data, for 5, 10, 20, and 40 nm thick ALD HfO$_2$ films. All MOCVD HfO$_2$ spectra (not shown) are similar to that of the polycrystalline 40 nm ALD HfO$_2$ sample. All MOCVD HfSiO spectra (not shown) are similar to that of the amorphous 5 nm ALD HfO$_2$ sample.

estimated uncertainty of 0.05 eV, are 5.88 eV for MOCVD polycrystalline HfO$_2$, 5.76 eV for MOCVD amorphous Hf-SiO, 5.75 eV for ALD polycrystalline HfO$_2$, and 5.62 eV for ALD amorphous HfO$_2$. The bandgap of the amorphous phase is slightly lower than that of polycrystalline phase. Our determined E_g is generally in good agreement with values measured by others, e.g., 5.25 eV to 5.8 eV for HfO$_2$.[18–20] The admixture of 20% Si, i.e., formation of hafnium silicate, leaves the bandgap largely unaffected within the experimental uncertainty.

Band edge defect states E_{def} are located 0.2–0.3 eV below the band-gap energy E_g. Interestingly, such states are observed if and only if the dielectrics exhibit crystallinity as detected by IR, XRD, and VUV-SE. This lends direct experimental support to a recent claim by Lucovsky *et al.*[21] They suggested that localized states below the metal *d*-state derived conduction-band edge in transition metal (and rare-earth) oxide films (sometimes observed by optical and x-ray absorption spectroscopy, and by photoconductivity measurements) originate from crystalline, but not from amorphous, material. Our data clearly support this assertion. However, it was also claimed that even "nanocrystalline" HfO$_2$ films, with a grain size <3 nm, exhibit such band edge states, although they appear amorphous in XRD.[21] Experimentally, we find that only "XRD crystalline" films exhibit band edge states.

In summary, we compare hafnium-based high-*k* dielectric films grown by MOCVD and ALD. MOCVD-grown HfO$_2$ films are mostly monoclinic, while HfSiO films are amorphous. Thin ALD-grown HfO$_2$ films are amorphous, while thick films are monoclinic, with traces of orthorhombic or tetragonal phase present. Sub-bandgap absorption is ob-

served in polycrystalline, but not in amorphous, films, lending direct experimental support to a recent claim by Lucovsky *et al.*[21] Finally, we note that sub-bandgap states discussed herein may be the underlying cause for gate leakage via Frenkel–Poole hopping. The addition of Si to HfO$_2$ reduces the tendency for crystallization, mitigating such issues. However, such sub-bandgap states will not likely be a limiting factor in high-*k*-based complementary MOS technologies, since they line up close to the band edge and are therefore not accessible at the low gate voltages employed.[22]

[1] G. D. Wilk, R. M. Wallace, and J. M. Anthony, J. Appl. Phys. **89**, 5243 (2001).
[2] G. D. Wilk, R. M. Wallace, and J. M. Anthony, J. Appl. Phys. **87**, 484 (2000).
[3] Z. Xu, M. Houssa, S. De Gendt, and M. Heyns, Appl. Phys. Lett. **80**, 1975 (2002).
[4] Y. S. Lin, R. Puthenkovilakam, and J. P. Chang, Appl. Phys. Lett. **81**, 2041 (2002).
[5] V. Rangarajan, H. Bhandari, and T. M. Klein, Thin Solid Films **419**, 1 (2002).
[6] Certain commercial equipment, instruments, or materials are identified in this paper in order to specify the experimental procedure adequately. Such identification is neither intended to imply recommendation or endorsement by the National Institute of Standards and Technology, nor is it intended to imply that the materials or equipment identified are necessarily the best available for the purpose.
[7] N. V. Nguyen, J.-P. Han, J. Y. Kim, E. Wilcox, Y. J. Cho, W. Zhu, Z. Luo, and T. P. Ma, *Characterization and Metrology for ULSI Technology: 2003 International Conference*, edited by D. G. Seiler, A. C. Diebold, T. J. Shaffner, R. McDonald, S. Zollner, R. P. Khosla, and E. M. Secula (American Institute of Physics, Melville, 2003), pp. 181–185.
[8] X. Zhao and D. Vanderbilt, Phys. Rev. B **65**, 233106 (2002).
[9] M. M. Frank, S. Sayan, S. Dörmann, T. J. Emge, L. S. Wielunski, E. Garfunkel, and Y. J. Chabal, Mater. Sci. Eng. B **109**, 6 (2004).
[10] D. A. Neumayer and E. Cartier, J. Appl. Phys. **90**, 1801 (2001).
[11] L. Koltunski and R. A. B. Devine, Appl. Phys. Lett. **79**, 320 (2001).
[12] D. Triyoso, R. Liu, D. Roan, M. Ramon, N. V. Edwards, R. Gregory, D. Werho, J. Kulik, G. Tam, E. Irwin, X.-D. Wang, L. B. La, C. Hobbs, R. Garcia, J. Baker, B. E. White, Jr., and P. Tobin, J. Electrochem. Soc. **151**, F220 (2004).
[13] M.-Y. Ho, H. Gong, G. D. Wilk, B. W. Busch, M. L. Green, P. M. Voyles, D. A. Muller, M. Bude, W. H. Lin, A. See, M. E. Loomans, S. K. Lahiri, and P. I. Räisänen, J. Appl. Phys. **93**, 1477 (2003).
[14] J. Aarik, A. Aidla, A.-A Kiisler, T. Uustare, and V. Sammelselg, Thin Solid Films **340**, 110 (1999).
[15] Y. J. Cho, N. V. Nguyen, C. A. Richter, J. R. Ehrstein, B. H. Lee, and J. C. Lee, Appl. Phys. Lett. **80**, 1249 (2002).
[16] S. Sayan, N. V. Nguyen, J. Ehrstein, T. Emge, E. Garfunkel, M. Croft, X. Zhao, D. Vanderbilt, I. Levin, E. P. Gusev, H. Kim, and P. J. McIntyre, Appl. Phys. Lett. **86**, 152902 (2005).
[17] A. S. Ferlauto, G. M. Ferreira, J. M. Pearce, C. R. Wronski, R. W. Collins, X. Deng, and G. Ganguly, J. Appl. Phys. **92**, 2424 (2002).
[18] P. Boher, P. Evrard, J. P. Piel, C. Defranoux, J. C. Fouere, E. Bellandi, and H. Bender, *Characterization and Metrology for ULSI Technology: 2003 International Conference*, edited by D. G. Seiler, A. C. Diebold, T. J. Shaffner, R. McDonald, S. Zollner, R. P. Khosla, and E. M. Secula, (American Institute of Physics, Melville, 2003), pp. 148–153.
[19] S.-G. Lim, S. Kriventsov, T. N. Jackson, J. H. Haeni, G. G. Schlom, A. M. Balbashov, J. L. Freeouf, and G. Lucovsky, J. Appl. Phys. **91**, 4500 (2002).
[20] V. V. Afanas'ev and A. Stesmans, Appl. Phys. Lett. **81**, 245 (2003).
[21] G. Lucovsky, C. C. Fulton, Y. Zhang, Y. Zou, J. Luning, L. F. Edge, J. L. Whitten, R. J. Nemanich, H. Ade, D. G. Schlom, V. V. Afanase'v, A. Stesmans, S. Zollner, D. Triyoso, and B. R. Rogers, IEEE Trans. Dev. Mater. Reliability (to be published).
[22] *International Technology Roadmap for Semiconductors* (Semiconductor Industry Association, San Jose, CA, 2004) ⟨http://public.itrs.net/⟩